



# The Influence of Different Influencing Factors in the Jointed Rock Formation on the Failure Mode of the Tunnel

Weijie Dong · Shenghu Ji · Chengqing Li ·  
Xu Chen · Yang Song

Received: 27 June 2022 / Accepted: 22 October 2022 / Published online: 1 November 2022  
© The Author(s), under exclusive licence to Springer Nature Switzerland AG 2022

**Abstract** The jointed surrounding rock is a geological condition that is frequently encountered during the construction of tunnels. The deformation and strength of jointed rock masses have an obvious anisotropy, and these mechanical properties could easily contribute to a number of factors, such as large deformation, collapse, initial support damage, and secondary lining cracking, during the construction process. Therefore, in this paper, the failure mode of the jointed rock is investigated, and the relationship between factors such as the dip angle of the joint, the joint spacing, the cover depth of the tunnel, and the stability of the jointed surrounding rock is explored with the help of the Shengli Tunnel. The results show that: (1) As the joint dip angle increases, the failure mode of the surrounding rock gradually evolves from flexural failure to shear-slip failure. (2) When the jointed spacing is between 0.5 and 2.0 m, the surrounding rock shows obvious anisotropy. As soon as it is greater than 2.0 m, the deformation of the surrounding rock decreases and the stability of the surrounding rock will be improved. (3) The increase in the surrounding

rock stress caused by the cover depth could result in a more significant unsymmetrical loading phenomenon. The yield area is primarily focused on the left arch shoulder and right arch foot, which should be supported and monitored during the excavation.

**Keywords** Jointed surrounding rock · Anisotropy · Failure mode · Numerical calculation

## 1 Introduction

Following the rapid development of transportation infrastructure in China, tunnel construction also evolves towards greater depths, longer distances and more complex geological conditions (Guo et al. 2021; Ren et al. 2019; Sun et al. 2017; Yin et al. 2018). It means that the difficulty of tunnel construction is rising.

Joint is one of the frequently encountered surrounding rock geologies in complex engineering geology (Deng et al. 2014; Do and Wu 2020; Qu et al. 2021; Wu et al. 2004). The interior of jointed rock masses usually contains a large number of weak structural surfaces, which cause the full rock mass to be cut into different smaller blocks. Layered structure due to lamellar planes, foliations, delamination and fractures enables the rock mass to exhibit significant anisotropy in physical and mechanical behaviour (Huang et al. 2013; Kim et al. 2012). During excavation, the rock would develop looseness and

---

W. Dong (✉) · S. Ji · C. Li · X. Chen  
Key Laboratory of Transportation Tunnel Engineering,  
Ministry of Education, Southwest Jiaotong University,  
Chengdu 610031, Si Chuan, China  
e-mail: 3498109394@qq.com

Y. Song  
Sichuan Lushi Expressway Co., Ltd, Chengdu, Si Chuan,  
China

be easily slid, dislodged, bent and fractured along the weak structural surfaces (Jia and Tang 2008). In some cases, the existence of joints could result in large deformations, collapses and other catastrophes in tunnel construction (Cao et al. 2018; Chen et al. 2019; Kulatilake et al. 2013). Therefore, it is essential to assess the stability of underground engineering in jointed rock masses.

The results of previous investigations have shown that a variety of factors such as spacing, dip and stiffness of joints could affect the mechanical properties of rock masses (Brown 1970; Brown and Trollope 1970; Reik and Zacas 1978; Yoshinaka and Yamabe 1986). In numerical simulations, methods for analysing laminated joint formations are mainly divided into continuum-based methods (Pouragha et al. 2018) and discontinuum-based methods. However, it seems difficult to explore qualitatively the effect of these factors on the mechanical properties of jointed rock masses.

Numerical method is an efficient and cost-effective tool for solving complex problems in rock engineering (Hoek 2001). Excavation of tunnels in jointed rock masses is an extremely complex and non-linear problem. Both experimental and theoretical methods have certain shortcomings in analysing the stability of jointed tunnels. Numerical simulations can quickly identify the most sensitive factors affecting the mechanical properties of the rock mass with powerful non-linear computational capabilities. The continuum and discontinuum modeling are two commonly used numerical approaches in rock engineering.

In continuum-based methods, layered structures in intact rock masses are usually modelled by assigning different material properties to mesh cells or adopting anisotropic models (Do et al. 2019; Fortsakis et al. 2012; Fossum 1985; Gerrard 1982; Ghaboussi et al. 1973). However, the continuum method is an implicit calculation method, which means that the rock material cannot be fractured or separated, and joints are limited to a small displacement level. It is different from the real damage state of the rock mass.

The distinct element method (DEM) is one of the popular methods for discontinuities (Cundall 1971, 1988; Hart et al. 1988), and it may be more appropriate for handling the behaviour of jointed rocks. The DEM models rock masses as a cluster of blocks which may be rigid or deformable and an explicit solution procedure is employed. The blocks are allowed to

behave as continuum media and the block and joint interactions are modelled by the Newton's laws of motion (Shreedharan and Kulatilake 2015). Fekete and Diederichs (2013) developed an intermittent model with 3DEC to simulate the failure of tunnels in massive rock masses. Xing et al. (2018) used the distinct element method to study the effects of the post-failure constitutive parameters of the rock masses, the mechanical properties of faults and the delayed supporting on tunnel stability. In the research of Shreedharan and Kulatilake (Shreedharan and Kulatilake 2015), the stability of two different shapes of tunnels in deep coal mines in China was investigated using 3DEC. Gu et al. (2020) investigated tunnel deformation using udec and concluded that complex ground stresses, easily weakened rock properties, asymmetric rock structure and uniform supporting structure are primary reasons that the roadway is asymmetrically deformed. Hu et al. (2021) investigated the role of stress ratios, slenderness ratios, rock orientation and rock layers considering the direction of excavation on the large deformation and depth of damage of the excavation by using the apparent element method (DEM).

There are some limitations to applying the existing results directly to engineering, due to the special and non-repeatable nature of underground engineering. Hence, it is necessary to investigate separately for Shengli Tunnel.

In this paper, the damage mechanism of jointed rock masses is firstly described, and then the influence of joint layer thickness, joint dip angle, tunnel depth and other factors on tunnel stability is qualitatively analysed by using the dem method based on the Victory Tunnel. This study can provide a basis for tunnel excavation and supporting.

## 2 Engineering Background

The Luding-Shimian Expressway spans across Luding County and Shimian County of Sichuan Province, China (Fig. 1a). It is an important part of the transportation plan in Sichuan Province.

Shengli Tunnel studied in this paper is one of the important control projects of the Lushi Expressway (Fig. 1b). The starting point of Shengli Tunnel is located in Zanli Village, Luqiao County (Fig. 1b). It passes through the typical mountain topography and

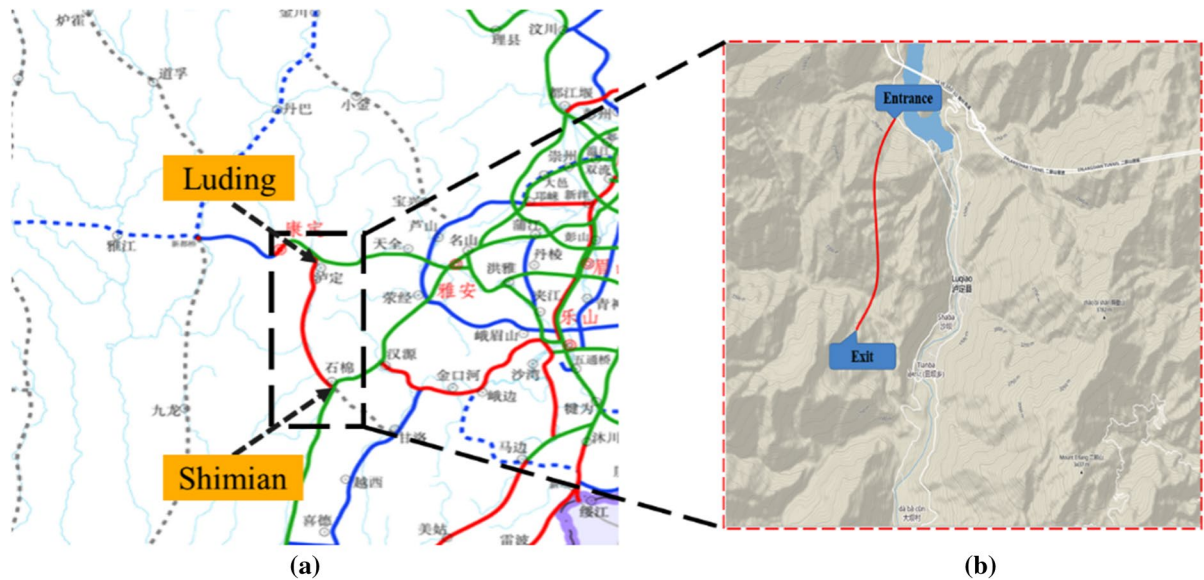


**Fig. 1** Location of the Shengli tunnel

extends to Gancao Village, Tianba County (Fig. 1b). The tunnel has a total length of 5 km, and the average section area is  $120 \text{ m}^2$ , while the maximum section area is  $140 \text{ m}^2$ .

Wide distribution of joints in the mileage section of Shengli Tunnel is from K500m to K600m. Preliminary survey and drilling data from the site indicate that the tunnel bedrock is primarily the underlying bedrock of the Upper Triassic (Fig. 2). The tunnel bedrock is exposed on the steep slope of the hillside and on both banks of the Dadu River. The main lithology consists of dark gray and black silty sericite slate, while the interior contains gray bands, medium-thick metamorphic cuttings and quartz sandstone interbedded with unequal thickness, sand slate interbedded with unequal thickness, and others. Diabase vein intrusions exist locally, while a large number of Cenozoic faults developed inside. The main fracture structures that affect the formation of the tunnel are the major fracture (F1) and the minor fracture (F2). Secondary faults are developed in the fault zone, with the lens structure being particularly prominent. The fault zone is mainly composed of slate, mudstone, and others, with obvious flaky structure, strip structure, and layered structure. After excavation, the rock at the tunnel face presented a layered distribution (Fig. 2c–f). The strata strike corresponded to the advancement direction of the tunnel face, which was consistent with the previous geological drilling data. Comparing figures d, e and f, it can be

seen that there are some differences in the thickness of the joints and the dip angle in all three images. The statistical results of the field investigation indicate that the actual rock thickness of the palm face ranges from 0.5 to 1.0 m, and there is a possibility that the layer thickness increases when crossing fault F1.

According to the previous experience of tunnel construction in this area, the tunnel excavation process of the layered joint fault section is susceptible to bias pressure, large deformations, collapse, and other phenomena. Therefore, in order to ensure the safe excavation of the Shengli Tunnel, the stability of the joint rock tunnel should be studied.

### 3 Mechanism of Deformation

This paper investigates the tunnel deformation in jointed rock, and statistics the formation lithology, the maximum stress of the original rock stress field, the compressive strength of the surrounding rock, the dip angle of joint, the maximum deformation, and the maximum deformation site. Some cases are shown in Table 1 (Meng et al. 2022).

According to the above statistics, when tunnelling in jointed rock, the stability of the surrounding rock is not only influenced by the joint dip angle, the strength of structural plane, and the force conditions, but also by the

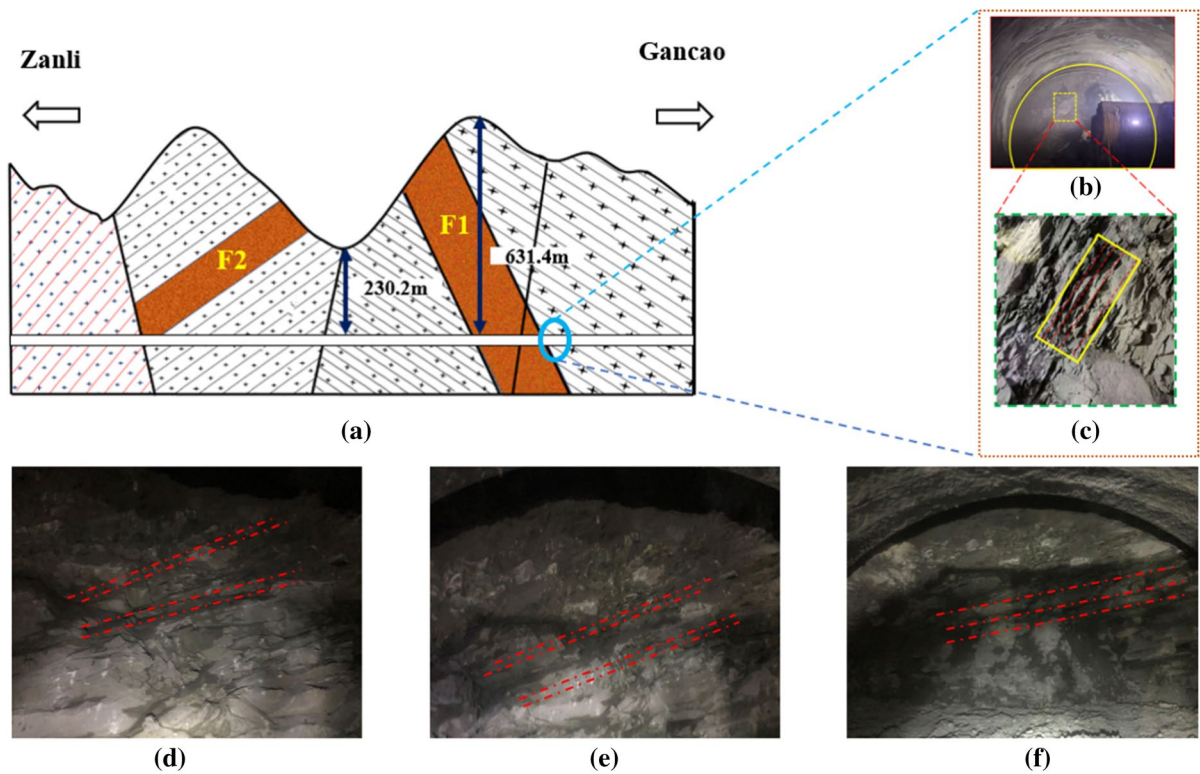


**Fig. 2** Profile of the Shengli tunnel

spacing, Layered structure, and orientation. In addition to the general surrounding rock deformation and failure characteristics of the tunnel, the deformation and failure of the surrounding rock masses are more complex due to the existence of structural planes or weak interlayers, and their manifestations are more diverse. From the form that jointed surrounding rock is destroyed, it is possible to classify the deformation failure of a jointed surrounding rock into two types, that is, flexural failure and shear-slip failure.

### 3.1 Shear Slip Failure

**Failure mechanism:** There are structural planes in jointed rock. After the tunnel excavation, the initial stress state of the surrounding rock varies. As soon as the stress state is ensured that the shear stress on the structural planes is greater than the shear strength, the structural plane is damaged.

The surrounding rock undergoes shear slip failure as shown in Fig. 3a, and the surrounding rock is stressed as shown in Fig. 3b. A schematic diagram of

a laminated rock mass containing a group of structural planes is shown in Fig. 3c. In this failure pattern,  $\beta$  is the angle between the minimum principal stress and the structural plane, and the stress on the structural plane is expressed as follows. As a calculation process, the normal stress and shear stress of layered rock mass are calculated by using the 2-1 and 2-2 formulas, and then equation 2-3 which is Mohr coulomb criterion is used to judge the stress state of layered rock mass.

$$\sigma = (\sigma_1 + \sigma_3)/2 + (\sigma_1 - \sigma_3) \cos 2\beta/2 \quad (2-1)$$

$$\tau = (\sigma_1 - \sigma_3) \sin 2\beta/2 \quad (2-2)$$

$$\tau = \sigma \tan \varphi + c \quad (2-3)$$

Condition for destabilization damage to tunnel sidewalls is as follows.

**Table 1** Deformation statistics of some typical layered jointed rock mass tunnels

Name	Rock softness	Maximum principal stress value (MPa)	Compressive strength of surrounding rock (MPa)	Joint dip angle (°)	Maximum deformation (mm)	Relative deformation (%)	The max deformation site
Ganban tunnel	Soft rock contains hard rock	23.9	14.1	62	398	4	Vault
Dujiashan tunnel	Soft rock contains hard rock	27.3	6.8	72	900	9	Vault
Maoyushan tunnel	Soft rock	22	5.6	80	1200	12	Vault
Guanjiao tunnel	Soft rock	22	13.8	70	405	4.1	Side wall
Zhifang tunnel	Hard rock contains soft rock	25	6	30	700	7	Bottom
Taoen tunnel	Soft rock	27.5	1.7	75	1200	12	Side wall
Tongsheng tunnel	Soft rock	20	4	35	841	8.4	Vault
Hadapu tunnel	Soft rock contains hard rock	12.6	6	0	650	6.5	Side wall
Wushaoling tunnel	Soft rock	32.2	1.7	29	1000	10	Side wall
Maoxian tunnel	Soft rock contains hard rock	27.5	2	75	810	8.1	Vault
Aerbeige tunnel	Soft rock	13	1.7	75	600	6	Side wall
Liangshui tunnel	Soft rock	25	2.9	65	750	7.5	Side wall
Suanshuiwan tunnel	Soft rock	16.6	5	60	710	7.1	Side wall
Beier tunnel	Soft rock contains hard rock	11	5	60	540	5.4	Side wall
Wuduxi tunnel	Soft rock contains hard rock	11.5	5	60	520	5.2	Side wall
Zhegushan tunnel	Soft rock	23.6	5.6	70	600	6	Vault
Longxi tunnel	Hard rock contains soft rock	27	15	68	512	5.1	Vault
Wenchuan No. 1 Tunnel	Soft rock	19.6	12	30	342	3.4	Bottom

$$\sigma_1 > \sigma_3 + 2(c + \sigma_3 \tan \varphi) / (1 - \tan \varphi \tan \beta) \sin 2\beta \tag{2-4}$$

where  $\sigma$  is the stress on the structure surface,  $\sigma_1$  is the maximum principal stress in the surrounding rock,  $\sigma_3$  is the minimum principal stress in the surrounding rock,  $\beta$  is the angle between the joint surface and the minimum principal stress,  $\varphi$  is the angle of internal friction at the surface, and  $c$  is the cohesive force at the surface.

After the tunnel is excavated, once the surrounding rock meets the stress relationship of Formula (2) to Formula (4), the side wall of the tunnel becomes unstable and breaks.

### 3.2 Flexural Failure

Failure mechanism: After tunnel excavation, a bending surface would be formed. With the help of secondary stresses in the surrounding rock, the jointed rock is subjected to tensile stress on the side which is close to the tunnel surface. Usually, the tensile strength of rock mass is generally far less than its compressive strength. Once the stress in the surrounding rock is greater than its tensile strength, flexural failure would occur.

The flexural failure of jointed rock is shown in Fig. 4a. The failure pattern of jointed rock is similar to that of the fixed beam, so the stress conditions when the



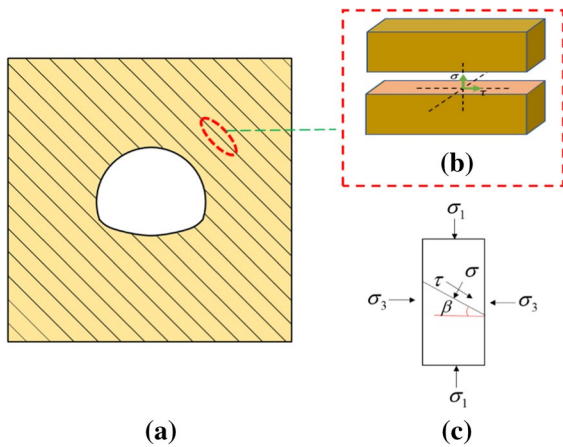


Fig. 3 Shear-slip failure of the surrounding rock

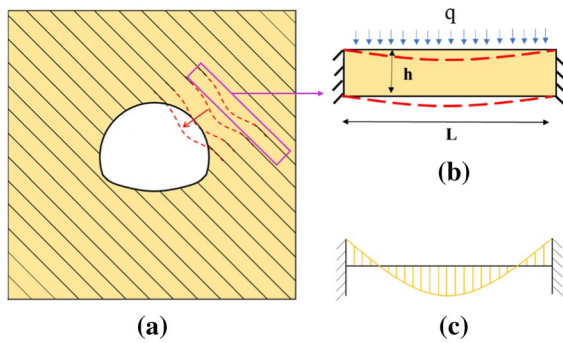


Fig. 4 Flexural failure of the surrounding rock

bending failure occurs in the surrounding rock can be analyzed with the fixed beam. Figure 4c is the bending moment diagram of the calculation model. From the figure, we can see that the maximum bending moment occurs in the central part of the beam.

$$M_{\max} = ql^2/12 \tag{2-5}$$

$$\sigma_{\max} = My/I = M_{\max}y/I = \gamma l^2/2h^2 \tag{2-6}$$

where  $q$  is the uniform stress,  $l$  is the length of beam slab,  $\gamma$  is the weight of rock formation, and  $h$  is the thickness of rock formation.

When the tensile strength of the surrounding rock  $\sigma < \sigma_{\max}$ , the surrounding rock maintains a stable state. Otherwise, if  $\sigma > \sigma_{\max}$ , the flexural failure of the surrounding rock occurs.

Flexural failure of the surrounding rock is mainly induced by unloading rebound, which occurs mainly in the rock body with high ground stress (such as deep burial or tunnels with high horizontal stress). It is always most prominent on the cavity wall, which intersects vertically with the initial maximum stress in the surrounding rock mass.

After tunnel excavation, when the thin laminated rock layer is almost perpendicular to the initial maximum stress, the surrounding rock is easily damaged under the rebound stress and eventually collapses by squeezing into the cavity.

### 4 Numerical Simulation

The calculation is carried out in the 3DEC software. A three-node triangular cell is selected to discretize the model, and an encrypted mesh is applied to the rock near the tunnel cross-section. The initial ground stress of the tunnel only takes into account the gravitational field, and the tunnel excavation is simulated according to the full-section excavation.

We adopt the mechanical parameters of Shengli tunnel as a reference for the numerical simulation in this paper. The geological parameters and structural plane parameters for this simulation are shown in Table 2.

The size of the tunnel cross-section is shown in Fig. 5. The cross-section of the tunnel is approximately 12 m wide and approximately 15 m high. Since the

Table 2 Related mechanical parameters of surrounding rock

Type	Volumetric weight (kN/m <sup>3</sup> )	Elastic modulus (GPa)	Poisson's ratio	Cohesive force (MPa)	Angle of internal friction (°)	Tensile strength (MPa)	Normal stiffness (Mpa)	Tangential stiffness (Mpa)
Sounding rock	25	20	0.25	1.50	50	0.8	–	–
Structural plane	–	–	–	0.08	19	–	30,000	3000

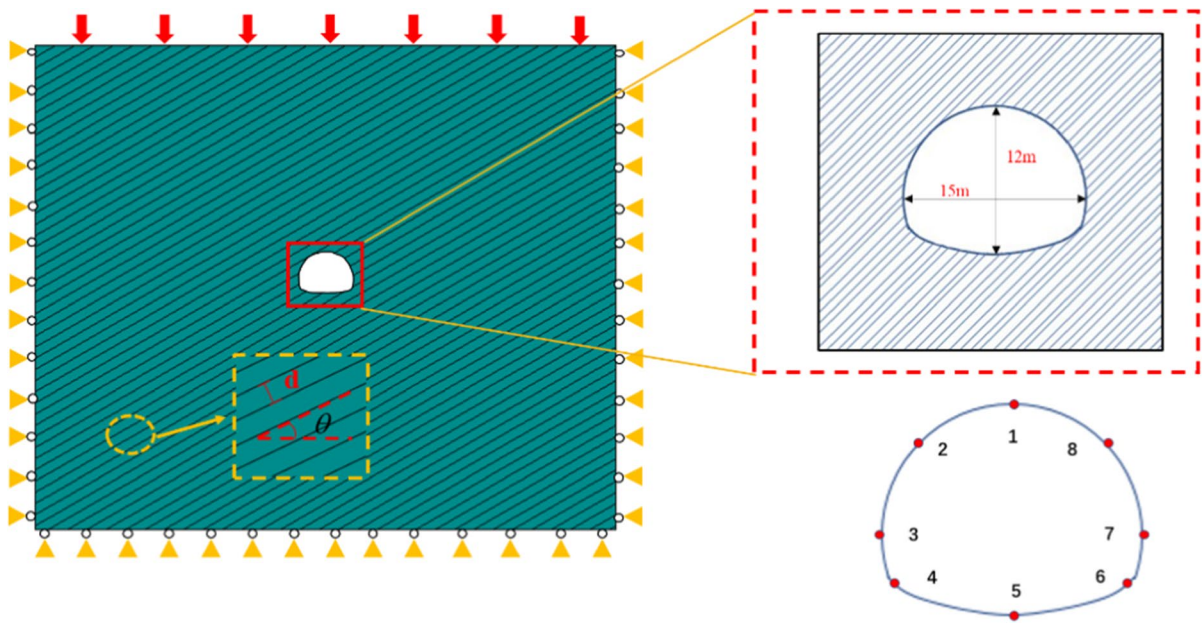


**Fig. 5** Calculation model

calculation results would be influenced by the scope of the model, the size of the model should be determined before anything else to ensure an accurate simulation. According to relevant research, the width of this simulation model is 120 m and the height 100 m. The simulation model of the tunnel is shown in Fig. 5, where measurement points for monitoring are placed around the perimeter of the tunnel, as shown in Fig. 5.

Constraints: In the numerical simulation, the boundary conditions are that vertical constraint applied at the bottom, the pressure applied at the top, the horizontal constraint applied at the left and right sides, and the side pressure coefficient is taken with reference to Eq. (1).

$$\lambda = \nu / 1 - \nu \tag{1}$$

where  $\lambda$  is the lateral pressure coefficient of the surrounding rock, and  $\nu$  is the Poisson’s ratio of the surrounding rock.

## 5 Results and Discussion

### 5.1 Influence of the Dip Angle of the Joints on the Stability of the Surrounding Rock

In practice, the tunnel crosses a wide area and the dip angle of the jointed rock is variable. Therefore, for a quantitative analysis and to study the influence of the joint dip angle on the stability of the surrounding rock, it is necessary to control the variation of the joint dip angle. The specific engineering conditions applied for the analysis are shown in Table 3.

**Table 3** Simulation parameters of different inclination angles

Engineering conditions	Joint dip angle (°)	Cover depth (m)	Joint spacing (m)
Condition 1	0	250	1.0
Condition 2	15	250	1.0
Condition 3	30	250	1.0
Condition 4	45	250	1.0
Condition 5	60	250	1.0
Condition 6	70	250	1.0

The displacement of the surrounding rock caused by tunnel excavation under different dip of jointed rock mass is shown in Fig. 6.

From Fig. 6a–f, it can be seen that joint would affect the deformation of the surrounding rock. When the dip angle of joints is  $0^\circ$ , the deformation of the surrounding rock is symmetrically distributed with the tunnel axis as the center. The maximum deformation is perpendicular to the direction of the joints, and it is located at the vault with a displacement value of 15.64 mm. As the joint dip angle increases from  $15^\circ$  to  $30^\circ$ ,  $45^\circ$ ,  $60^\circ$ , and  $75^\circ$ , the maximum deformation of the surrounding rock gradually becomes parallel to the joint direction, and the displacement value changes from 15.62 to 18.12 mm, 15.37 mm, 21.39 mm, and 25.16 mm. During this process, the deformation of the surrounding rock on both sides of the tunnel gradually shows differences, and the location where the maximum deformation occurs gradually shifts from the vault to the left arch shoulder.

The maximum principal stress distribution of the surrounding rock under different dip angles is shown in Fig. 7. When the joint dip angle is

small, the surrounding rock resembles a "superimposed beam". After excavation of the tunnel, an empty surface is formed, and the surrounding rock at the vault has formed flexural failures, as shown in Fig. 7a, b. As the joint dip angle increases, the stress required to trigger flexural failure of the surrounding rock gradually increases, while the stress required to trigger shear-slip failure decreases. As the joint dip angle increases to a specific value, the stresses required to trigger flexural failure and shear-slip failure of the surrounding rock of the joint are equal. At this time, the maximum deformation direction of the surrounding rock is at a certain angle with the joint, as shown in Fig. 7d. After the joint dip angle exceeds a certain value, the instability of surrounding rock is dominated by shear slip failure, and the maximum deformation is parallel to the joint plane, as shown in Fig. 7e, f.

The relationship between the deformation of the key points of the surrounding rock and the dip angle is shown in Fig. 8. From Fig. 8, it can be seen that there is a difference in the response of the vault and the arch bottom to the joint dip angle. The deformation

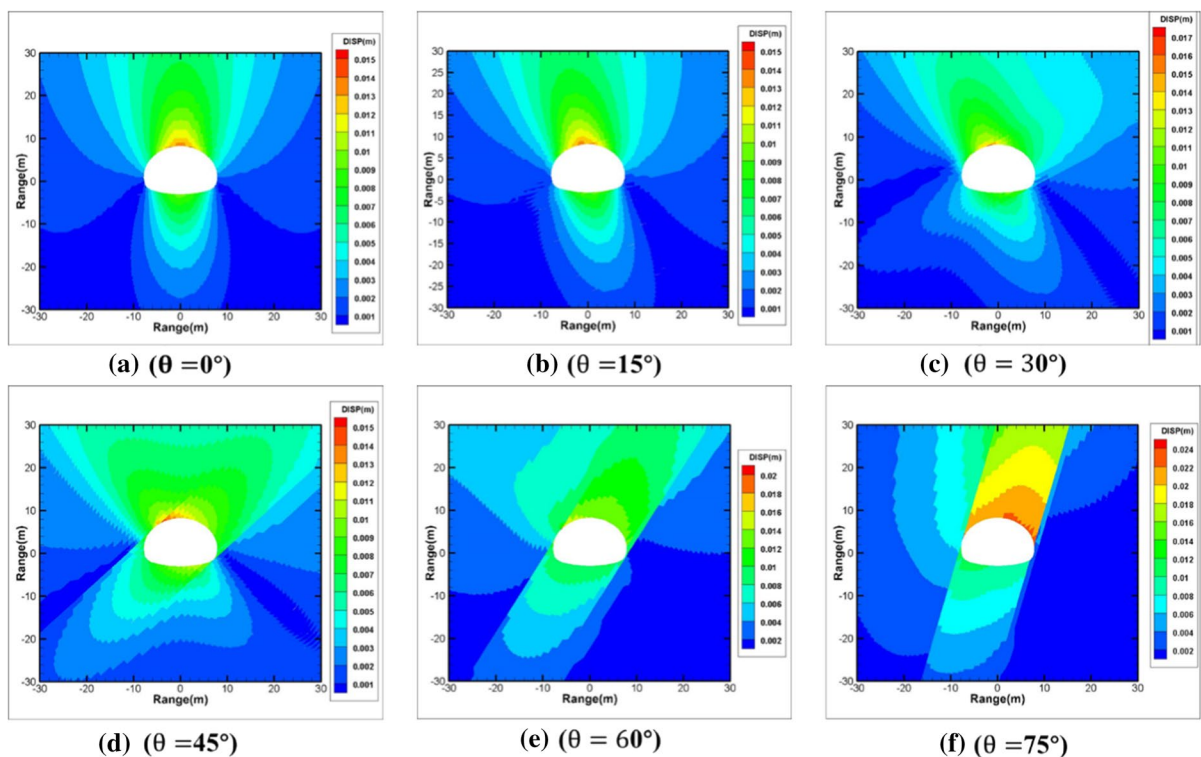


**Fig. 6** Deformation of surrounding rock under different joint dip angles



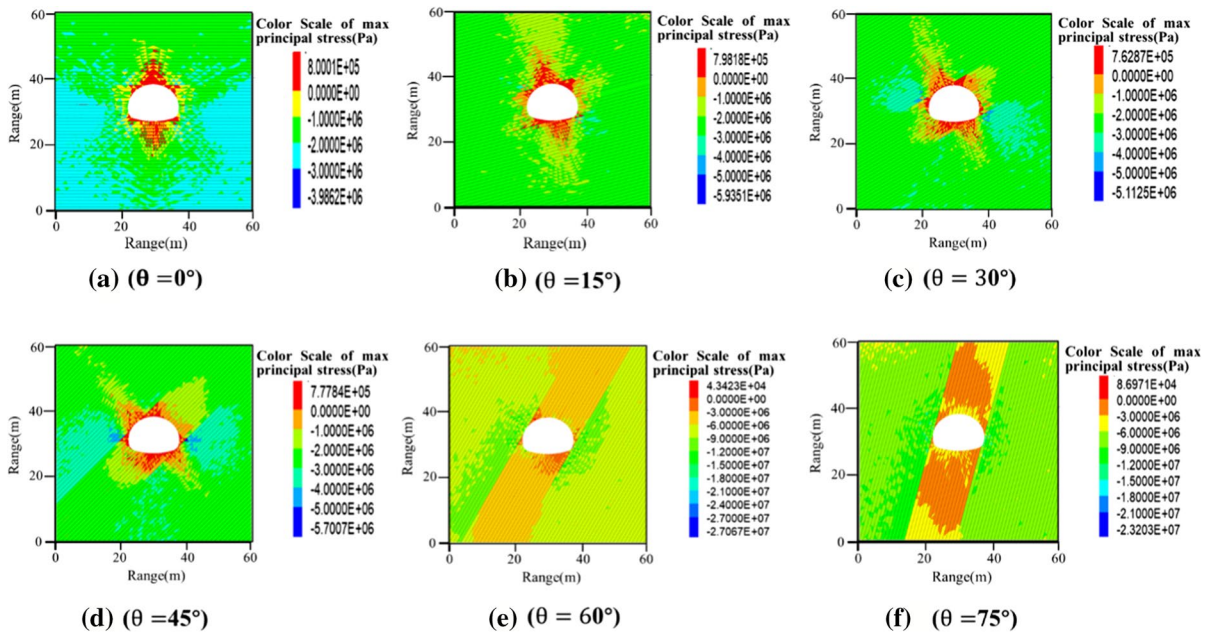


**Fig. 7** Maximum principal stress distribution under different joint dip angles

at the bottom of the arch fluctuates within a certain value when the joint dip angle changes.

As for the vault, when the joint dip angle increases from 0° to 60°, the deformation of the surrounding rock fluctuates within a certain range. However, as soon as the joint dip angle increases from 60° to 75°, the deformation of the vault increases rapidly. The relationship between the deformation of the arch shoulder and the fluctuations in the joint dip angle is shown in Fig. 8. As the joint dip angle increases, the deformation at the right arch shoulder decreases before increasing. The deformation of the left arch shoulder increases between 0° and 15°, but the deformation tends to level off between 15° and 45° and increases rapidly after 45°.

The radial stress after tunnel excavation is much greater than the normal stress of the surrounding rock. When the joint dip angle is between 0° and 30°, as the joint dip angle increases, the angle between the radial stress of surrounding rock and the joint plane continues to increase at the right arch shoulder. It increases the stress required by the joint surface for the occurrence of shear failure, resulting in a decrease in deformation. When the joint dip angle is greater than 30°, as the angle of inclination of the joint increases, the angle between the radial stress and the joint face

continues to decrease, the stress required for shear failure decreases, and the stress in the direction parallel to the joint face increases, which as a result, easily form shear failure, making the deformation increase and gradually parallel to the direction of the joint. When the joint dip angle is between 0° and 45°, the surrounding rock at the left arch shoulder is mainly damaged by compression bending. With the change of the inclination angle, the normal stress at the left shoulder and the length of the "equivalent superimposed beam" will both change, which causes the deformation of the surrounding rock to first increase and then decrease. When the dip angle exceeds 45°, shear damage predominates in this area. The failure mechanism is similar to that at the right arch shoulder, where the deformation increases with increasing dip angle.

When the dip angle of the joint is 0, the area where plastic deformation occurs at the vault and bottom is deeper than other areas (Fig. 9a). At this time, the yield zone is mainly perpendicular to the joint, and the surrounding rock appears to have been damaged by flexural failure. As the dip angle changes, the yield zone gradually spreads from the top of the arch to the depth of the arch shoulder, and there is a large yield zone both perpendicular to the joint and parallel to

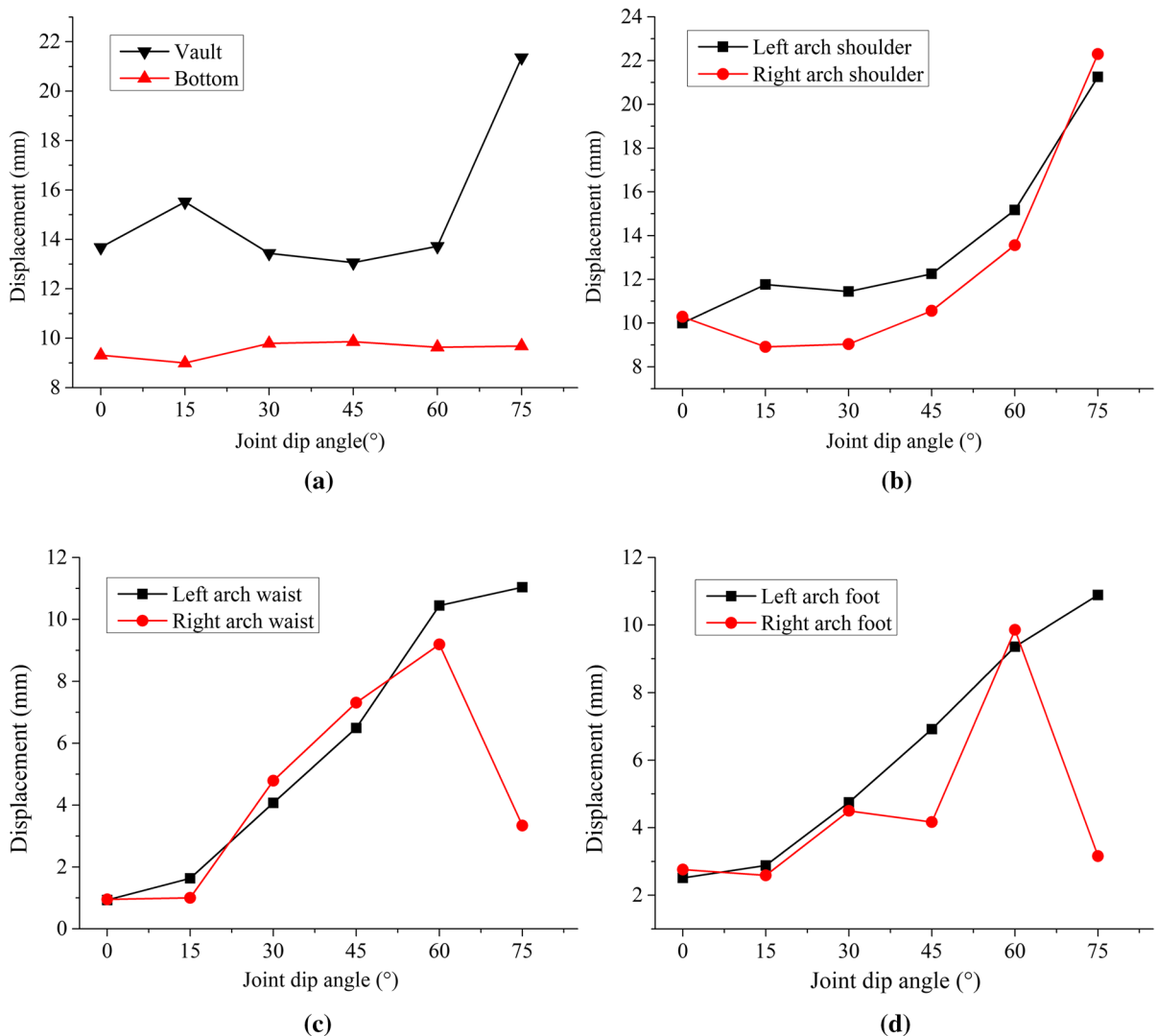


**Fig. 8** Influence of joint dip angles on surrounding rock deformation

the joint direction. It is mainly explained that there are two patterns of shear-slip failure and compression-bending failure in the surrounding rock at this stage. After this stage, the yielding zone is mainly parallel to the joint face, and shear slip failure is the most common occurrence.

## 5.2 The Effect of Joint Spacing

The influence of joint spacing is inevitable in the analysis of the mechanical properties of the surrounding rock. The surrounding rock mechanics under different joint spacing are quite different. Therefore, in

order to investigate the influence of joint spacing on the mechanical behavior of the surrounding rock after tunnel excavation, an analysis was carried out according to the engineering conditions shown in Table 4.

The deformation of the surrounding rock during tunnel excavation with different joint spacing is shown in Fig. 10. Since the jointed spacing is 0.5 m, the maximum deformation of the surrounding rock is at the left arch shoulder, where the maximum deformation value is 25.32 mm. Thereafter, as the layer spacing increases to 1 m, 2 m, 3 m, 4 m, and 5 m, the deformation value of the surrounding rock changes accordingly to 15.94 mm, 12.78 mm, 10.42 mm,

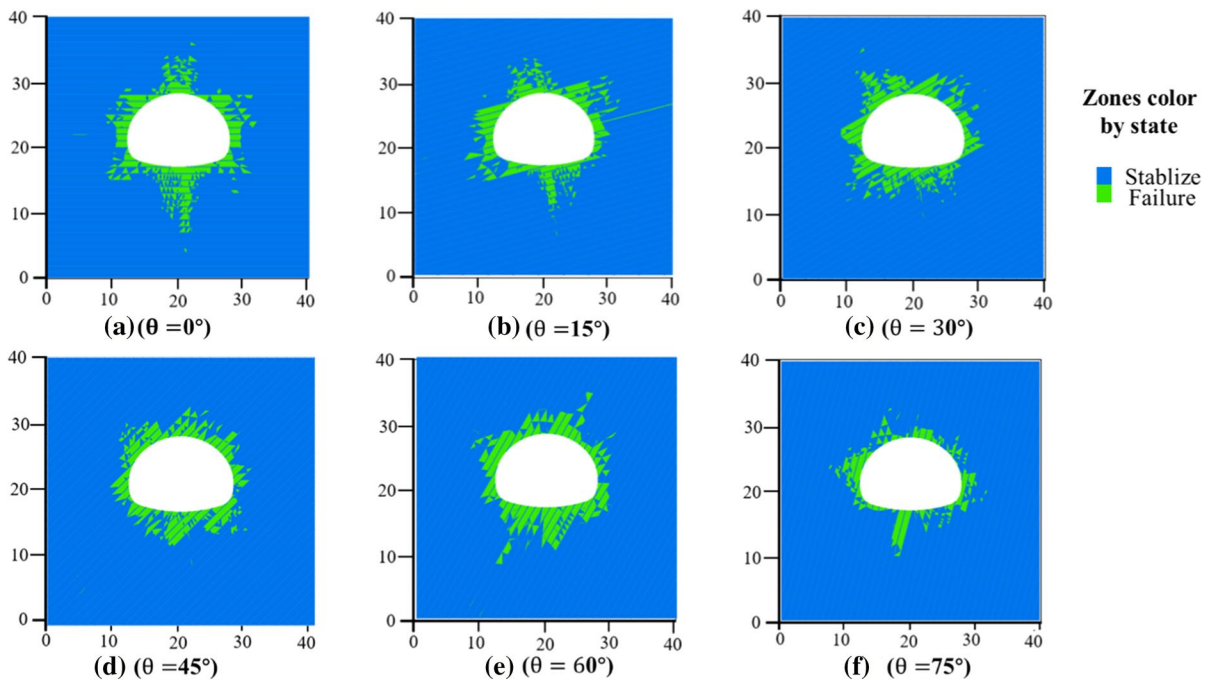


**Fig. 9** Distribution of yield zone with different joint dip angles

**Table 4** Values of related parameters for different rock layer thicknesses

Condition	Joint spacing (m)	Joint dip angle (°)	Cover depth (m)
1	0.5	45	250
2	1.0	45	250
3	2.0	45	250
4	3.0	45	250
5	4.0	45	250
6	5.0	45	250

10.97 mm, and 8.65 mm. However, the position of maximum deformation is always between the arch shoulder and the vault area. During the tunnel excavation process, this area should be monitored.

The maximum principal stress distribution of the surrounding rock under different rock layer thicknesses is shown in Fig. 11. When the layer thickness is 0.5 m, the maximum principal stress in the surrounding rock is 0.8 MPa. As the layer thickness increases from 1 to 5 m, the maximum principal stress of the surrounding rock continuously decreases. According to Formula (2) to Formula (6), as the layer

thickness  $h$  increases, the shape and size of the tunnel section remain unchanged, that is, when the other parameters of the formula remain unchanged, the principal stress in the surrounding rock decreases, improving the ability to withstand bending damage. At the same time, the increase in the layer thickness is equivalent to reducing the number of structural surfaces, and the possibility of a shear failure of structural surfaces is reduced.

As in the previous subsection, the deformation of key areas of the tunnel was monitored during the excavation, and the results obtained are shown in Fig. 12. The deformation at the vault and arch bottom varies with the joint spacing, as shown in Fig. 12a. The deformation at the vault decreases from 16.76 to 10.76 mm as the layer joint spacing increases from 0.5 to 2 m, and the deformation at the bottom also decreases from 13.49 to 7.32 mm, which changes significantly. After the thickness exceeds 2 m, the deformation continues to decrease, and the deformation rate decreases significantly.

Comparing Fig. 12b with Fig. 12a and c, it can be seen that the deformation of the surrounding rock at the arch shoulders is more sensitive to the variation of the joint spacing than other areas. As the joint spacing

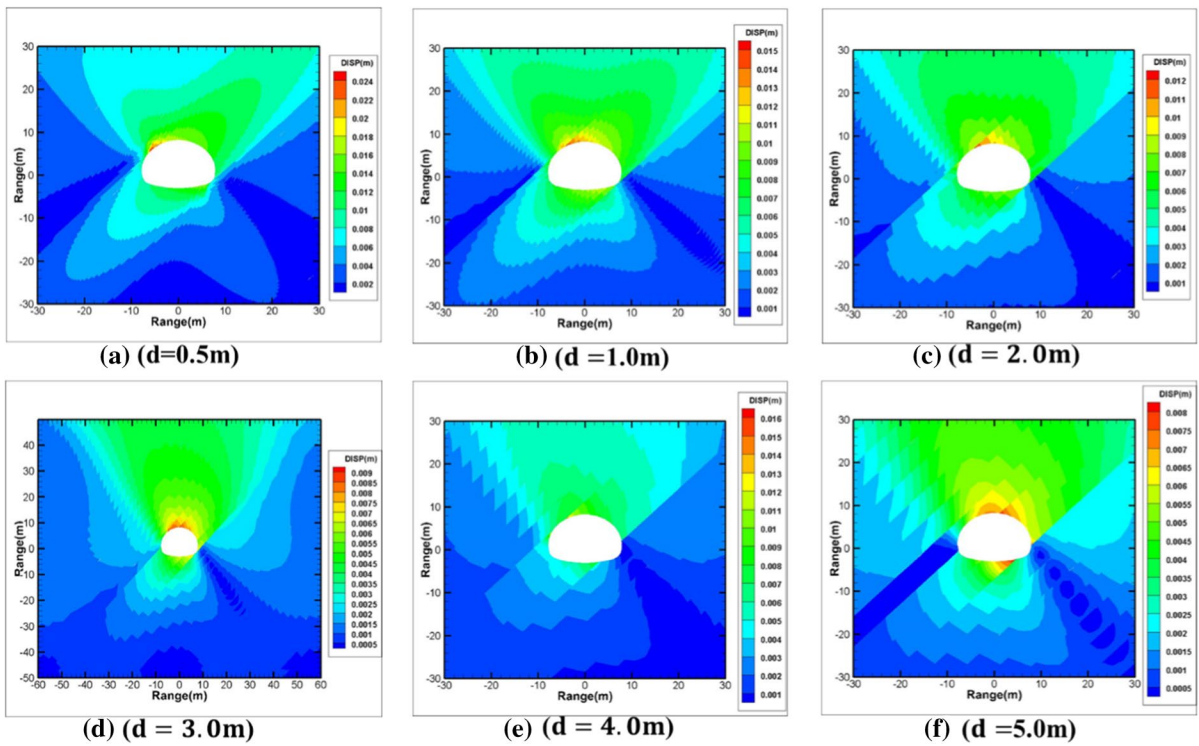


**Fig. 10** Influence of joint spacing on tunnel deformation

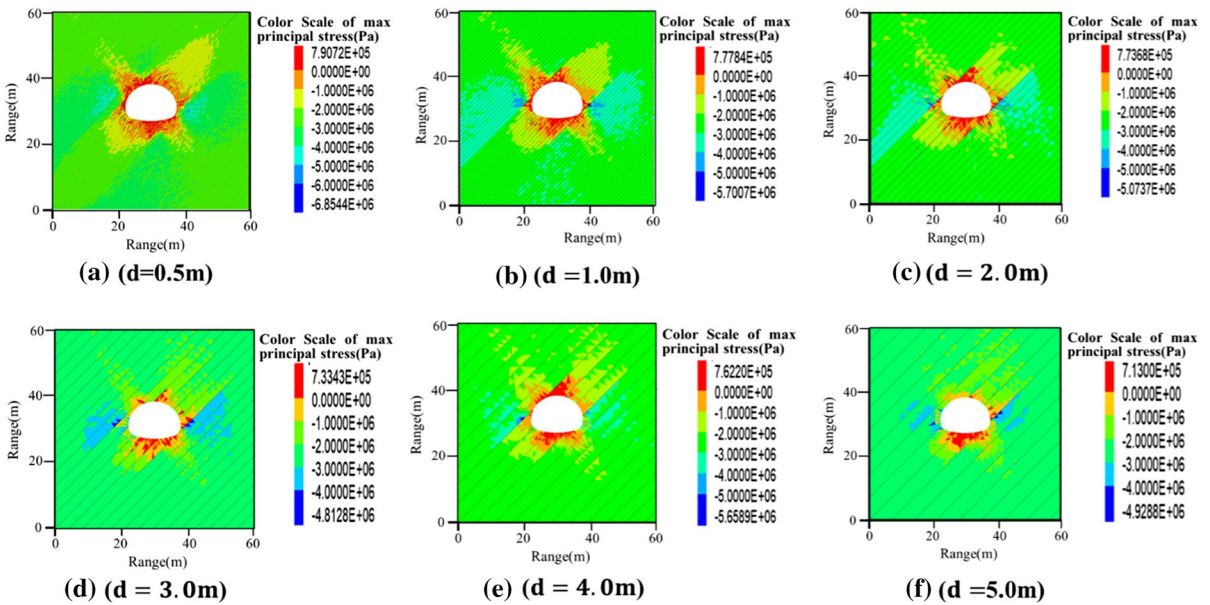


**Fig. 11** Distribution of maximum principal stress with different joint spacing



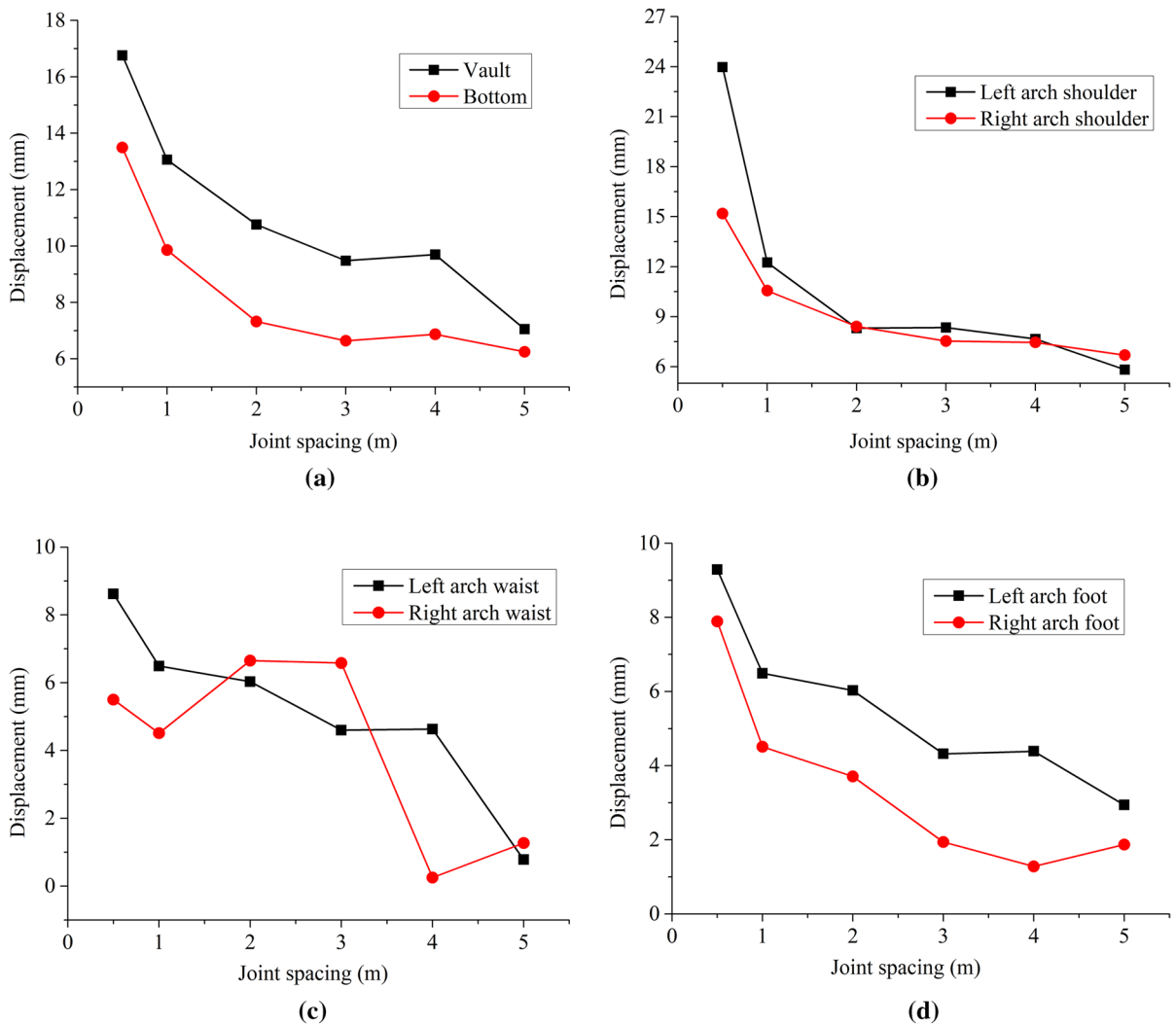


**Fig. 12** Displacement of monitoring points under different joint spacing

increases from 0.5 to 2 m, the deformation at the left and right arch shoulders decreases to 11.72 mm and 4.62 mm, respectively. Subsequently, the deformation trend of the surrounding rock in this area is similar to that in Fig. 12a. As the thickness increases, the deformation and its rate continue to decrease.

With regard to the arch waist area, there is an obvious difference between the left and right sides as the joint spacing increases. After the tunnel is excavated, the surrounding rock on the left is prone to shear failure and bending failure. As the joint spacing increases, the resistance of the surrounding rock to deformation increases, thereby showing the same trend as the other areas. The reason that

the deformation of the surrounding rock at the right arch waist increases with a thickness of 2 m to 3 m is attributed to the proximity of the monitoring point to the joint plane, where the deformation is influenced by the joint plane.

Figure 13 shows the plastic zone of the surrounding rocks with different thicknesses. It can be seen that the yield area is distributed in the direction perpendicular to and parallel to the joints when the joint spacing is 0.5 m, while the distribution is concentrated at the left arch shoulder and right arch foot. As the joint spacing increases, the yield area of the surrounding rock decreases, especially in the direction perpendicular to the joint. Once joint spacing

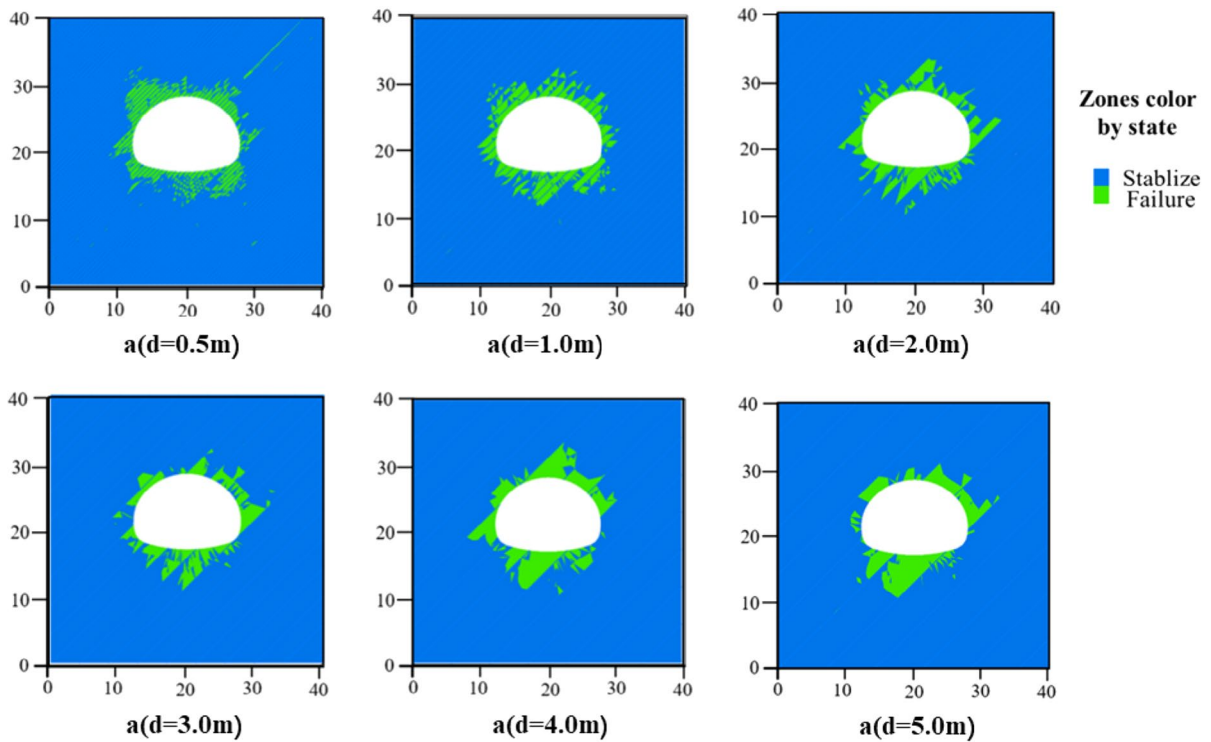


**Fig. 13** Yield area of surrounding rock under different joint spacing

increases to 5 m, the yield area at the right arch foot is almost negligible. It is mainly explained by the increased integrity of the surrounding rock due to the growth of joint spacing, and the ability to resist flexural failure and shear failure is enhanced. Therefore, the growth of joint spacing enhances the stability of the surrounding rock and facilitates tunnel excavation.

### 5.3 The Influence of Depth on the Stability of Surrounding Rock

Cover depth is an important factor that influences the stability of the tunnel surrounding rock during the tunnel excavation. Therefore, it is necessary to classify the depth in intervals of 100 m for the purposes of fully understanding the influence of the cover depth on the stability of the tunnel excavation. The specific engineering conditions are shown in Table 5.

The deformation of the surrounding rock at different depths is shown in Fig. 14. At a depth of 250 m, the maximum deformation around the tunnel occurs between the arch shoulder and the vault, and its value is 18.12 mm. As cover depth increases from 350 to

**Table 5** Values of related parameters under different buried depths

Condition	Cover depth (m)	Joint dip angle (°)	Joint spacing (m)
1	250	50	1.0
2	350	50	1.0
3	450	50	1.0
4	550	50	1.0
5	650	50	1.0
6	750	50	1.0

750 m, the greatest deformation of the surrounding rock does not change significantly. They are all between the spandrel and the dome, but the deformation value increases from 23.16 to 73.51 mm. It can be seen that there is an approximately linear change between the maximum deformation of the surrounding rock and cover depth.

The maximum principal stress distribution of the surrounding rock under different cover depths is shown in Fig. 15. As the depth increases from 250

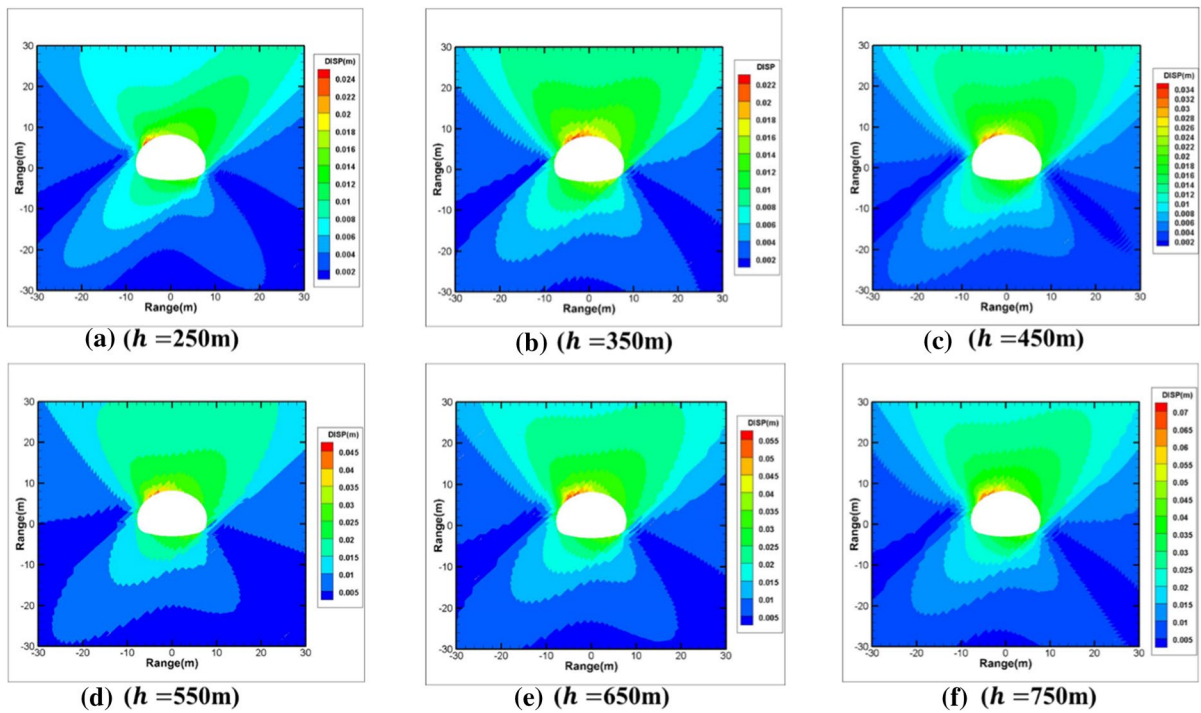


**Fig. 14** Influence of cover depth on surrounding rock deformation

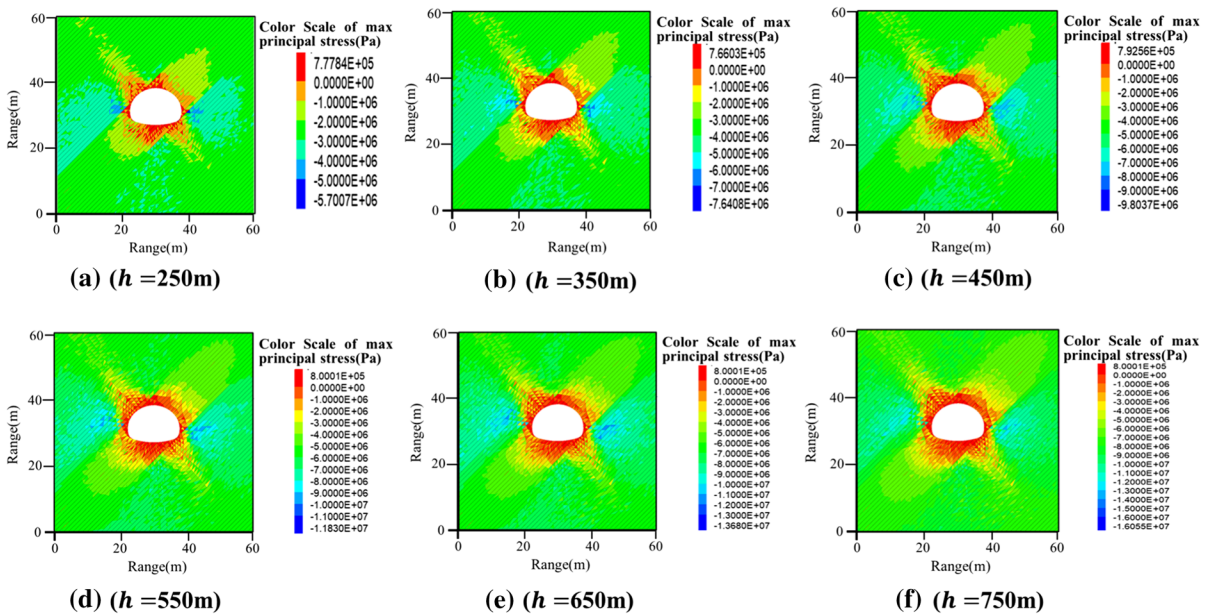


**Fig. 15** Distribution of maximum principal stress with different cover depth

to 750 m, the stress increases from 0.78 to 0.8 MPa. When the properties of the surrounding rock do not change, the shear strength of the surrounding rock is considered to be unchanged. As the buried depth increases, the principal stress increases. When the ratio of the principal stress to the shear strength exceeds a certain value, the surrounding rock will be destroyed. Therefore, increasing the buried depth will reduce the stability of the surrounding rock.

The relationship between depth and deformation of key parts around the cave can be explored, and the monitoring results are shown in Fig. 16. As the depth increases, the deformation of each monitoring point increases, but there is a certain difference in the

growth rate. Figure 16a shows the relationship curve of the vault, the arch bottom, and the cover depth. It can be seen from the figure that at the same depth, the deformation at the vault is greater than that at the bottom, and as the depth increases, the difference between the deformation of the vault and the bottom of the arch tends to expand. Figure 16b shows the deformation as the cover depth varies at the sidewall. Due to the presence of joints, the deformation on the left and right arch shoulders is different. And as the buried depth increases, both the deformation amount and the rate of deformation are greater at the left arch shoulder than at the right arch shoulder. This phenomenon is attributed to the more uneven distribution

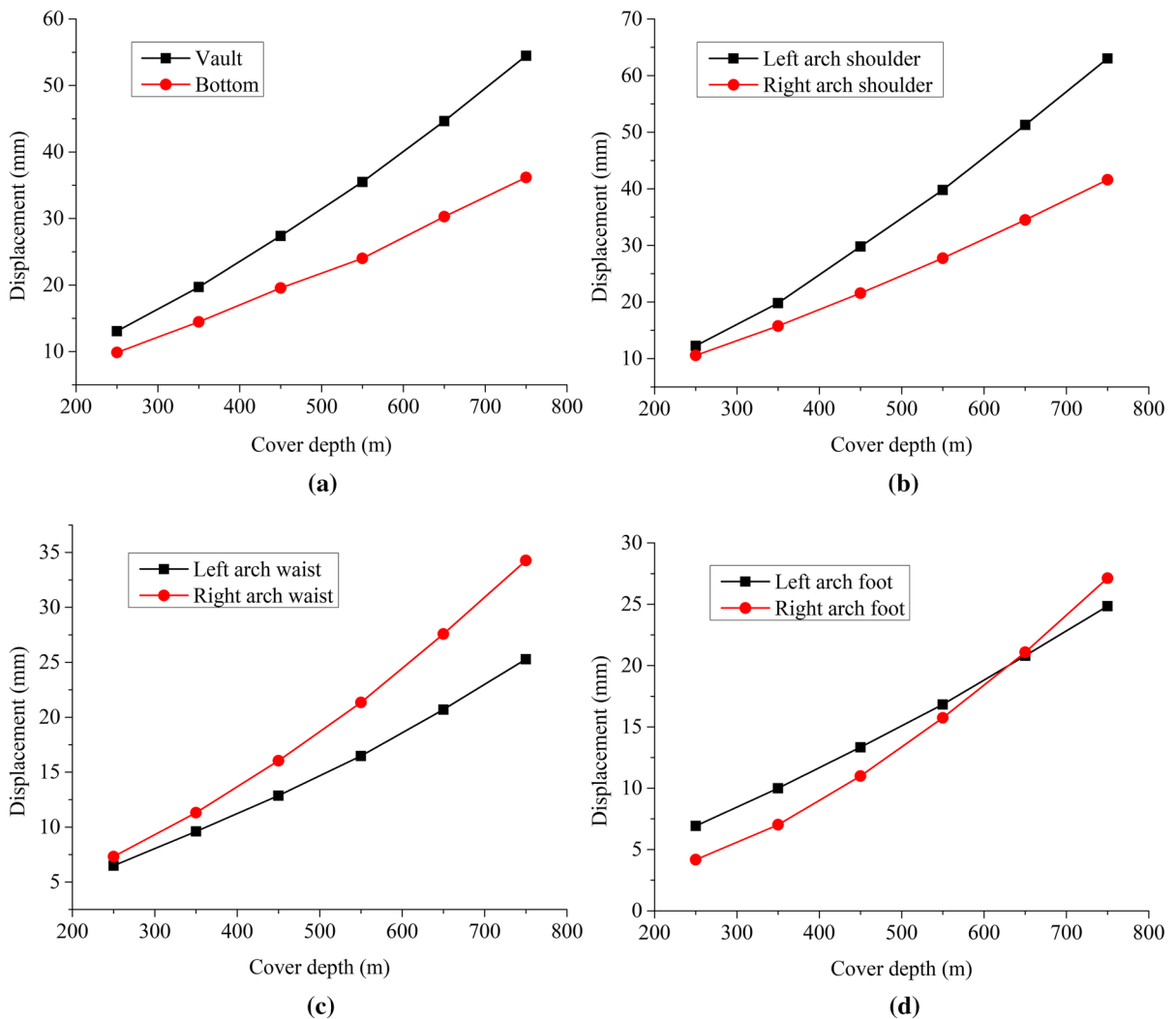


**Fig. 16** Displacement of monitoring points at different cover depth



of the deflective stresses generated by the jointed envelope as the depth increases, resulting in different deformations on each side. Figure 16d shows the deformation of the surrounding rock at the arch foot. While the depth varies from 250 to 650 m, the deformation at the left arch foot is always greater than that at the right arch foot, but the difference between them decreases as the depth increases. When the cover depth is 650 m, the change in the surrounding rock is the same on the left and right sides. Accordingly, the growth of depth could exacerbate the asymmetric deformation of the left and right arches of the tunnel.

It can be seen that with the increase of depth, there is a tendency for the deflection of the surrounding rock to increase (Fig. 16). Meanwhile, the change in depth has a significant impact on the left arch shoulder and the right arch foot. It is mainly caused by the fact that this area is not only subject to compression bending failure but also to shear slip deformation. As a result, targeted measures should be taken in this location in deeply buried tunnels.

According to Fig. 17, the plastic zone of the surrounding rock is smaller when the buried depth is 250 m, and the plastic zone gradually increases as

the buried depth increases. This is mainly due to the increase in the buried depth of the tunnel and the increase in the surrounding rock stress around the tunnel, which in turn leads to an increase in the amount of deformation required for stress release after the tunnel is excavated, and an increase in the extent of the plastic zone and the depth of spread.

### 6 Conclusion

The Shengli Tunnel served as the background for the project to investigate the relationship between the joint dip angle, the jointed spacing, the cover depth of the tunnel, and the stability of the surrounding rock. The conclusions are as follows.

- (1) The presence of joints allows for an unequal stress distribution on both sides of the tunnel. In the hard-jointed surrounding rock, the mechanical mechanism of surrounding rock failure would change with the different dip angles. When the angle is small, the surrounding rock failure is dominated by flexural failure, which

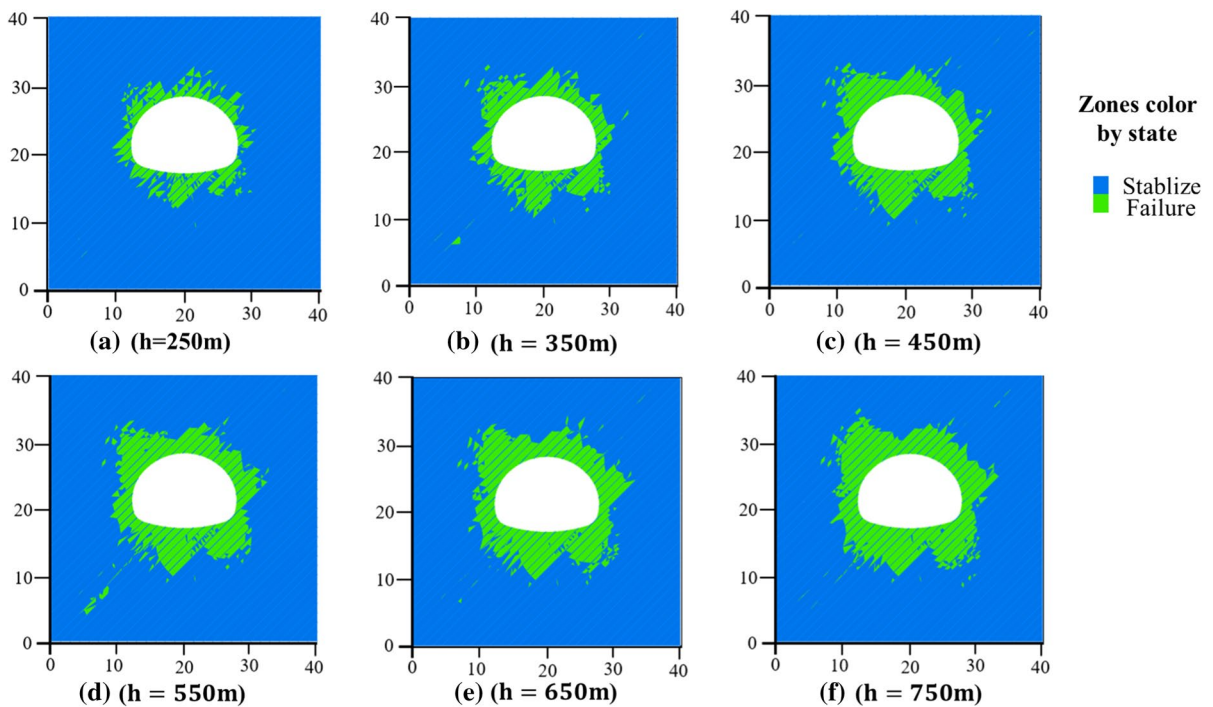


**Fig. 17** Influence of cover depth on the distribution of yield zones in the tunnel surrounding rock

is mainly concentrated at the vault. As joint dip angle increases, the shear-slip failure gradually becomes significant. Once the angle exceeds  $60^\circ$ , failure is dominated by shear-slip damage.

- (2) It is the variation of the joint spacing which directly influences the stability of the surrounding rock. As the thickness increases, the deformation of the surrounding rock decreases and its stability increases. When the thickness of the joints is small ( $d < 2$  m), the anisotropic effect of the surrounding rock after tunnel excavation is significant due to the relatively dense joints. Once joint spacing exceeds 2 m, the mechanical properties of the rock block tend to be that of a complete rock mass, and the deformation of the surrounding rock is small, which is conducive to tunnel excavation and support.
- (3) The influence of depth on the stresses in the jointed envelope has similarities to normal rock formations. In other words, an increase in depth increases the stress and deformation around the tunnel. The variation of depth has the greatest effect on the deformation at the vault area. As the depth increases, there is a high risk of the plastic extrusion failure at vault, which could trigger phenomena such as falling blocks. The difference to the normal surrounding rock is that the jointed surrounding rock will create a bias pressure phenomenon, which brings about an obviously asymmetrical distribution of stresses and deformations on both sides of the tunnel axis. The greater the depth, the greater the deviations.

The research in this paper focuses exclusively on the damage mechanisms and influencing factors of tunnels with high-ground stress jointed rock environments. In addition, the support system and deformation control techniques need to be further researched.

**Author Contributions** All authors contributed to the study conception and design. Material preparation, data collection and analysis were performed by WD, SJ and CL. All authors read and approved the final manuscript.

**Funding** This research was supported by the funding from the National Natural Science Foundation of China (51808459).

**Data Availability** All data, models and code generated or used during the study appear in the submitted article are available from the corresponding author by request.

## Declarations

**Conflict of interest** The authors declare that they have no known competing financial interests or personal relationships that could have appeared to influence the work reported in this paper.

## References

- Brown ET (1970) Strength of models of rock with intermittent joints. *J Soil Mech Found Div* 96:1935–1949
- Brown ET, Trollope DH (1970) Strength of a model of jointed rock. *J Soil Mech Found Div* 96:685–704
- Cao C, Shi C, Lei M, Yang W, Liu J (2018) Squeezing failure of tunnels: a case study. *Tunn Undergr Space Technol* 77:188–203. <https://doi.org/10.1016/j.tust.2018.04.007>
- Chen Z, He C, Xu G, Ma G, Wu D (2019) A case study on the asymmetric deformation characteristics and mechanical behavior of deep-buried tunnel in phyllite. *Rock Mech Rock Eng* 52(11):4527–4545. <https://doi.org/10.1007/s00603-019-01836-2>
- Cundall PA (1971) A computer model for simulating progressive, large-scale movements in blocky rock systems
- Cundall PA (1988) Formulation of a three-dimensional distinct element model—part I. A scheme to detect and represent contacts in a system composed of many polyhedral blocks. *Int J Rock Mech Min Sci Geomech Abstr* 25:107–116
- Deng XF et al (2014) Numerical study on tunnel damage subject to blast-induced shock wave in jointed rock masses. *Tunn Undergr Space Technol* 43:88–100. <https://doi.org/10.1016/j.tust.2014.04.004>
- Do TN, Wu J-H (2020) Simulation of the inclined jointed rock mass behaviors in a mountain tunnel excavation using DDA. *Comput Geotech* 117:103249. <https://doi.org/10.1016/j.compgeo.2019.103249>
- Do N-A et al (2019) Behavior of noncircular tunnels excavated in stratified rock masses—case of underground coal mines. *J Rock Mech Geotech Eng* 11:99–110. <https://doi.org/10.1016/j.jrmge.2018.05.005>
- Fekete S, Diederichs MS (2013) Integration of three-dimensional laser scanning with discontinuum modelling for stability analysis of tunnels in blocky rockmasses. *Int J Rock Mech Min Sci* 57:11–23
- Fortsakis P, Nikas K, Marinos V, Marinos P (2012) Anisotropic behaviour of stratified rock masses in tunnelling. *Eng Geol* 141:74–83
- Fossum AF (1985) Effective elastic properties for a randomly jointed rock mass. *Int J Rock Mech Min Sci Geomech Abstr* 22:467–470
- Gerrard CM (1982) Elastic models of rock masses having one, two and three sets of joints. *Int J Rock Mech Min Sci Geomech Abstr* 19:15–23
- Ghaboussi J, Wilson EL, Isenberg J (1973) Finite element for rock joints and interfaces. *Int J Rock Mech Min Sci Geomech Abstr* 11:66
- Gu C, Xu Q, Yang H, Fang X, Xue G (2020) Asymmetric deformation mechanism and control of roadway in structural complex area. *Geotech Geol Eng* 39:145–155

- Guo Z et al (2021) Geomechanical model experiment study on deformation and failure mechanism of the mountain tunnel in layered jointed rock mass. *Adv Civ Eng* 2021:1–19. <https://doi.org/10.1155/2021/6645124>
- Hart RD, Cundall PA, Lemos JV (1988) Formulation of a three-dimensional distinct element model—part II. Mechanical calculations for motion and interaction of a system composed of many polyhedral blocks. *Int J Rock Mech Min Sci Geomech Abstr* 25:117–125
- Hoek E (2001) Big tunnels in bad rock. *J Geotech Geoenviron Eng* 127:726–740
- Hu B, Sharifzadeh M, Feng X, Guo W, Talebi R (2021) Role of stress, slenderness and foliation on large anisotropic deformations at deep underground excavations. *Int J Min Sci Technol* 31:577–590
- Huang F, Zhu H, Xu Q, Cai Y, Zhuang X (2013) The effect of weak interlayer on the failure pattern of rock mass around tunnel—scaled model tests and numerical analysis. *Tunn Undergr Space Technol* 35:207–218. <https://doi.org/10.1016/j.tust.2012.06.014>
- Jia P, Tang CA (2008) Numerical study on failure mechanism of tunnel in jointed rock mass. *Tunn Undergr Space Technol* 23:500–507
- Kim H, Cho J-W, Song I, Min K-B (2012) Anisotropy of elastic moduli, P-wave velocities, and thermal conductivities of Asan Gneiss, Boryeong Shale, and Yeoncheon Schist in Korea. *Eng Geol* 147–148:68–77. <https://doi.org/10.1016/j.enggeo.2012.07.015>
- Kulatilake PHSW, Wu Q, Yu Z, Jiang F (2013) Investigation of stability of a tunnel in a deep coal mine in China. *Int J Min Sci Technol* 23(4):579–589. <https://doi.org/10.1016/j.ijmst.2013.07.018>
- Meng L, et al (2022) An improved classification method of asymmetrical squeezing large deformation of layered soft rock tunnels under high geo-stresses. *Chinese J Rock Mech Eng* 41(1):147–156
- Pouragha M, Wan R, Eghbalian M (2018) Critical plane analysis for interpreting experimental results on anisotropic rocks. *Acta Geotech* 14:1215–1225
- Qu T, Wang Z, Zhao W, Pan K (2021) Research on meso-mechanism of failure mode of tunnel in jointed rock mass. *Geotech Geol Eng* 39(6):4329–4339. <https://doi.org/10.1007/s10706-021-01761-8>
- Reik G, Zacas M (1978) Strength and deformation characteristics of jointed media in true triaxial compression. *Int J Rock Mech Min Sci Geomech Abstr* 15:295–303
- Ren F, Zhu C, He M (2019) Moment tensor analysis of acoustic emissions for cracking mechanisms during schist strain burst. *Rock Mech Rock Eng* 53(1):153–170. <https://doi.org/10.1007/s00603-019-01897-3>
- Shreedharan S, Kulatilake PHSW (2015) Discontinuum-equivalent continuum analysis of the stability of tunnels in a deep coal mine using the distinct element method. *Rock Mech Rock Eng* 49:1903–1922
- Sun X-M et al (2017) Physical modeling of floor heave for the deep-buried roadway excavated in ten degree inclined strata using infrared thermal imaging technology. *Tunn Undergr Space Technol* 63:228–243. <https://doi.org/10.1016/j.tust.2016.12.018>
- Wu J-H, Ohnishi Y, Nishiyama S (2004) Simulation of the mechanical behavior of inclined jointed rock masses during tunnel construction using discontinuous deformation analysis (DDA). *Int J Rock Mech Min Sci* 41(5):731–743. <https://doi.org/10.1016/j.ijrmms.2004.01.010>
- Xing YY, Kulatilake PHSW, Sandbak L (2018) Effect of rock mass and discontinuity mechanical properties and delayed rock supporting on tunnel stability in an underground mine. *Eng Geol* 238:62–75
- Yin Q, Jing H, Ma G, Su H, Liu R (2018) Investigating the roles of included angle and loading condition on the critical hydraulic gradient of real rock fracture networks. *Rock Mech Rock Eng* 51(10):3167–3177. <https://doi.org/10.1007/s00603-018-1526-x>
- Yoshinaka R, Yamabe T (1986) Joint stiffness and the deformation behaviour of discontinuous rock. *Int J Rock Mech Min Sci Geomech Abstr* 23:19–28

**Publisher's Note** Springer Nature remains neutral with regard to jurisdictional claims in published maps and institutional affiliations.

Springer Nature or its licensor (e.g. a society or other partner) holds exclusive rights to this article under a publishing agreement with the author(s) or other rightsholder(s); author self-archiving of the accepted manuscript version of this article is solely governed by the terms of such publishing agreement and applicable law.